Single-mode Condition and Bending Loss Analysis of Ultrafast Laser-inscribed Mid-infrared Waveguides in GeAsSe Chalcogenide Glass

Takashi Yasui

Faculty of Engineering
Kitami Institute of Technology, Kitami-shi, Hokkaido, 090-8507, Japan
yasui@mail.kitami-it.ac.jp

Abstract – In this study, single-mode conditions and bending losses of optical waveguides based on $Ge_{33}As_{12}Se_{55}$ chalcogenide glass, commercially known as IG2, for astrophotonic devices in the mid-infrared spectral range are numerically analyzed. The scalar finite-element method was used to analyze single-mode conditions. For the bending-loss analysis, equivalent straight waveguides of bent waveguides were analyzed using the two-dimensional finite-difference beam-propagation method. The results revealed design rules for astrophotonic optical integrated circuits in the mid-infrared spectral range.

Index Terms – Astrophotonics, beam-propagation method, bending-loss analysis, finite-element method, optical waveguide, single-mode condition.

I. INTRODUCTION

Optical integrated circuits (OICs), which are vital in current optical telecommunication systems, are being widely used in astrophysics to meet the astronomers' ever-increasing demand for higher angular, spectral, and temporal resolutions over a broad wavelength range among astronomers. Astronomers hope to understand the formation of planets, stars, and galaxies to characterize the atmospheres of exoplanets in habitable zones and unravel the physics of black holes. The application of the OICs in astronomy is referred to as astrophotonics. The OIC-based solutions have advantages in terms of size, weight, and cost compared to solutions based on conventional free-space optics. In addition, they can realize functionalities that are difficult or impossible to achieve using conventional solutions. Astrophotonics will be important in the new era of extremely large 30-m class telescopes [1, 2].

Various astrophotonic instruments have been developed [3–15]. Most of them are operated in the near-infrared (IR) spectral range owing to the availability of technologies in the field of optical telecommunications. However, astrophotonic instruments operating in the mid-IR spectral range have also been considered for the direct detection and characterization of exo-earths. Spectral features in the mid-IR range offer signatures of important chemicals in habitable zones such as water, ozone, and carbon dioxide [16, 17].

Chalcogenide glasses are promising materials for mid-IR OICs because of their broad transparency ranges. In addition, the ultrafast laser inscription (ULI) technique, which generates permanent refractive index changes, is a highly cost-effective and convenient method for inscribing waveguides in chalcogenide glasses [5, 11–15, 18]. The change in the refractive index due to ULI can be controlled by the pulse energy.

$Ge_{33}As_{12}Se_{55}$ chalcogenide glass, also known as IG2 [19], is a well-established chalcogenide composition commonly used in mid-IR applications [14, 15, 20]. Because IG2 glass is transparent from 1 μm up to 12 μm of the wavelength range [15] that covers the two atmospheric transmission windows (3-5 and 8-12μm), IG2 glass is suitable for astrophotonic OICs operated in mid-IR. Ultrafast laser-inscribed IG2 glass waveguides for mid-IR OICs, such as directional couplers with rectangular waveguides operating at a single wavelength, have been fabricated and demonstrated. Measured coupling ratio of a fabricated coupler was compared to the ones by an analytical and a numerical method[14]. Although characterizations such as the single-mode operation of the rectangular waveguides have been experimentally performed at a single wavelength, their single-mode condition has been theoretically analyzed only for square waveguides at a single wavelength [15].

Bent waveguides are important building blocks of OICs. Although bent waveguides with small radii are vital for realizing compact OICs, the losses that occur in bent waveguides increase as the bending radii decrease. A smaller bend loss is required for astrophotonic OICs because astronomical observation programs are inherently photon starved. However, to the best of our knowledge, the bending losses of ultrafast laser-inscribed IG2 glass waveguides have not been experimentally or theoretically characterized.

In this study, the analysis of single-mode conditions using the scalar finite-element method (FEM) [21] and bending-loss analysis using the two-dimensional finite-difference beam-propagation method (FD-BPM) [22] were carried out for IG2-glass-based waveguides. These results provide fundamental information for designing high-performance astrophotonic devices based on IG2 glass in the mid-IR spectral range.

II. CONFIGURATION AND NUMERICAL METHODS

A. Bent waveguides

We consider a bent waveguide shown in Fig. 1. The bent waveguide consists of a rectangular core, whose width, thickness, and refractive index are, respectively, w, t, and n_{core}. The core is surrounded by a cladding material with a refractive index of n_{clad}. It is assumed that two uniform straight waveguides, whose cores and claddings are identical to the ones of the bent waveguide, are connected to the input and output of the bent waveguide.

In this study, we assumed that the cladding material was IG2 glass, and that the core was fabricated using the ULI technique. The refractive index of the cladding, n_{clad}, is expressed as follows[19]:

$$n_{clad}^2(\lambda) = A + \frac{B_1\lambda^2}{\lambda^2 - C_1^2} + \frac{B_2\lambda^2}{\lambda^2 - C_2^2}, \quad (1)$$

where $A = 3.3408$, $B_1 = 2.9626$, $C_1 = 0.3600$, $B_2 = 0.8298$, and $C_2 = 35.0011$. The refractive index of the core is expressed as $n_{core} = n_{clad} + \Delta n$, where Δn denotes the refractive-index change by the ULI, whose range covers 0.008-0.02[15]. In this study, we considered the waveguides operated in E^x modes.
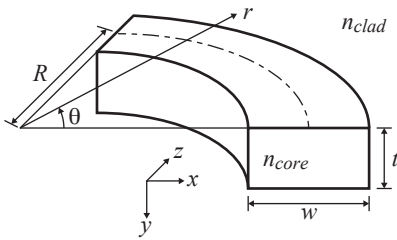

Fig. 1. Three-dimensional view of a bent waveguide, whose core is surrounded by a cladding material.

B. Brief review of FEM

In this section, we briefly review the scalar FEM. The scalar FEM is applied to analyze the single-mode condition of the straight waguides connected to the bent waveguide. We note that a single cross-section of the bent waveguide is necessary for the analysis. Suppose the cross-section is placed on the xy-plane. Under a scalar wave approximation, the following wave equation is derived from the Maxwell's equations:

$$p_F\frac{\partial^2\Psi}{\partial x^2} + p_F\frac{\partial^2\Psi}{\partial y^2} + q_F k_0^2\Psi - p_F\beta^2\Psi = 0, \quad (2)$$

where $\Psi = E_x$, $p_F = 1$, $q_F = n^2(x,y)$ for E^x modes, $\Psi = H_x$, $p_F = 1/n^2(x,y)$, $q_F = 1$ for E^y modes, and $n(x,y)$ denotes the cross-sectional refractive-index distribution.

After dividing the cross-section by the second-order triangular elements and applying the scalar finite-element method, the following finite-element equation was derived [21]:

$$[K]\{\Psi\} - k_0^2 n_{eff}^2[M]\{\Psi\} = \{0\}, \quad (3)$$

where $[K]$ and $[M]$ denote the finite-element matrices, $\{\Psi\}$ is the nodal electric/magnetic field vector, $\{0\}$ is the null vector, and k_0 and n_{eff} are, respectively, the wave number in vacuum and the effective refractive index. Here, n_{eff}^2 and $\{\Psi\}$ are, respectively, an eigenvalue and eigenvector of equation (3). The Neumann boundary condition is imposed on the computational window edges.

C. Two-dimensional equivalent straight waveguide

Figure 2 (a) shows an equivalent two-dimensional waveguide of the bent waveguide shown in Fig. 1. The refractive indices of the core and cladding are, respectively, denoted as n_{co} and n_{cl}, which are evaluated using the effective index method.

The bent waveguide can be mapped onto an equivalent straight waveguide (ESW), as shown in Fig. 2 (b), using a conformal transformation[23]. It is noted that the ESW is also applicable to cylindrical waveguides[24, 25]. Here, $u = R\ln\left(1 + \frac{q}{R}\right)$, $q = r - R$, and $s = R\theta$. The refractive index distribution of the ESW, $n'(u)$, is expressed as follows [23–27]:

$$n'(u) = n(q)\left(1 + \frac{q}{R}\right), \quad (4)$$

where, $n(q)$ denotes the refractive index distribution of the bent waveguide and is expressed as follows:

$$n(q) = \begin{cases} n_{co} & \left(-\frac{w}{2} \leq q \leq \frac{w}{2}\right) \\ n_{cl} & \text{(otherwise)} \end{cases}. \quad (5)$$

D. Brief review of FD-BPM

Herein, we briefly review the two-dimensional FD-BPM. We consider an ESW as shown in Fig. 2 (b). From Maxwell's equations, the following wave equation is obtained:

$$\frac{\partial}{\partial u}\left(p_B\frac{\partial\Phi}{\partial u}\right) + \frac{\partial}{\partial s}\left(p_B\frac{\partial\Phi}{\partial s}\right) + k_0^2 q_B\Phi = 0, \quad (6)$$

where, $\Phi = E_y$, $p_B = 1$, $q_B = n'^2(u)$ for the transverse electric (TE) modes, and $\Phi = H_y$, $p_B = 1/n'^2(u)$, $q_B = 1$ for the transverse magnetic (TM) modes.

Substituting the solution of the form:
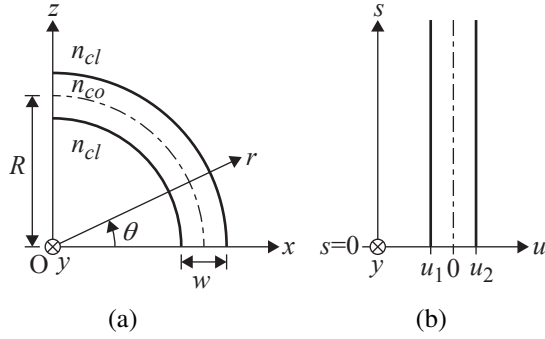
$$\Phi(u,s) = \varphi(u,s)\exp(-jk_0 n_0 s), \quad (7)$$

Fig. 2. (a) Two-dimensional bent waveguide and (b) its ESW for 2-D FD-BPM. Here, $u_1 = R\ln\left(1 - \frac{w/2}{R}\right)$ and $u_2 = R\ln\left(1 + \frac{w/2}{R}\right)$.

Fig. 3. Single-mode region for the IG2-glass-based waveguides with the refractive change, Δn, of 0.011 at a wavelength of 9 μm.

into equation (6), we obtain the following equation for the slowly varying complex amplitude φ:

$$p_B \frac{\partial^2 \varphi}{\partial s^2} - 2jk_0 n_0 p \frac{\partial \varphi}{\partial s} + \frac{\partial}{\partial u}\left(p_B \frac{\partial \varphi}{\partial u}\right)$$
$$+ k_0^2 (q_B - n_0^2 p_B)\varphi = 0, \quad (8)$$

where n_0 is the reference refractive index.

After applying the Padé approximation [28] and the finite-difference procedure, the following system of equations is derived [22]:

$$a_i^+ \varphi_{i-1}(s+\Delta s) + b_i^+ \varphi_i(s+\Delta s) + c_i^+ \varphi_{i+1}(s+\Delta s)$$
$$= a_i^- \varphi_{i-1}(s) + b_i^- \varphi_i(s) + c_{i+1}^- \varphi_{i+1}(s), \quad (9)$$

where a^+, b^+, c^+, a^-, b^-, and c^- are finite-difference coefficients; i represents values at the ith sampling point in the u-direction; and Δs denotes the propagation step size in the s-direction. equation (9) results in a system of N linear equations, when $\varphi_i(s)$ $(i = 1, 2, \ldots, N)$ are given. Here, N denotes the number of transverse sampling points. After solving equation (9), the propagating field of $\varphi_i(s+\Delta s)$ $(i = 1, 2, \ldots, N)$ are obtained. The transparent boundary condition[29] is used.

III. NUMERICAL RESULTS

A. Single-mode conditions

Figure 3 shows the boundary between single- and multi-mode regions for the rectangular waveguides with $\Delta n = 0.011$ at the wavelength of 9 μm evaluated by the FEM, where filled and open circles, respectively, represent single- and multi-mode operation. Hereafter, we consider square waveguides with $w = 15$ μm and $t = 15$ μm, and rectangular waveguides with $w = 20$ μm and $t = 15$ μm, which are operated in single mode.

Figure 4 shows the normalized propagation constant, $b = (n_{eff}^2 - n_{clad}^2)/(n_{core}^2 - n_{clad}^2)$, as a function of the wavelength for the square and rectangular waveguides with Δn of 0.09, 0.011, 0.013, and 0.015. Notably, no higher-order mode was found for each value of Δn
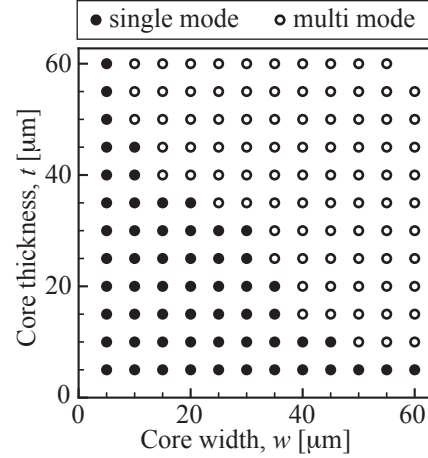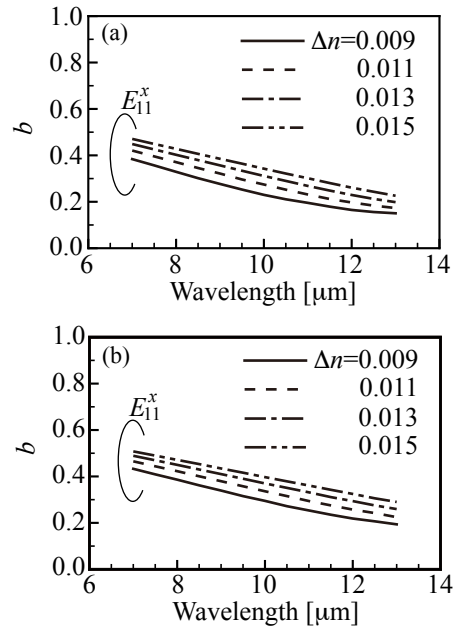

Fig. 4. Dispersion curves as a function of wavelength for waveguides with (a) $w = 15$ μm and $t = 15$ μm and (b) $w = 20$ μm and $t = 15$ μm. No higher-order mode was found in the wavelength range.

over the wavelength range. Evidently, the waveguides are operated in single mode over the wavelength range and in the range of Δn.

It was experimentally and numerically shown that square waveguides with $w = t = 15$ μm whose Δns were in the range from 0.0097 to 0.0142 were operated in a single mode at the wavelength of 7.8 μm [15]. We can see that Fig. 4 (a) shows the same tendency.

B. Bending loss analysis

The two-dimensional FD-BPM was employed to estimate the bending losses of the ESWs. The fundamental mode of the original two-dimensional straight waveguide with a refractive index distribution of $n(q)$ was launched in the ESWs at the $s = 0$. The distribution of the fundamental mode is given as an initial field of the BPM calculation, which are denoted $\varphi_i(0)$ $(i = 1, 2, \ldots, N)$ in equation (9). The spacing between transverse sampling points is $\Delta u = 0.1 \ \mu$m. The propagation step size $\Delta s = 5 \ \mu$m. The transverse computational window size was $100 \ \mu$m. A core of an ESW was placed in the center of the computational window. The pure bend loss (PBL) was evaluated using the steady-state differential power loss (DPL) level[30]. DPL was evaluated as follows [26, 31, 32]:

$$\Gamma(s) = -\frac{10}{\Delta s'} \log_{10} \left[\frac{P(s + \Delta s')}{P(s)} \right], \qquad (10)$$

where $P(s)$ denotes the modal power at s, estimated by the overlap integral between the incident and propagating fields [27], and s and $s + \Delta s'$ represent the two points used to estimate the modal power. In other words, PBL is the slope of the graph of $\log_{10}(P(s))$[22].

Figure 5 shows the bending radius and wavelength dependence of PBL on bent waveguides whose refractive index changes, Δn, are 0.11 with the square and rectan-
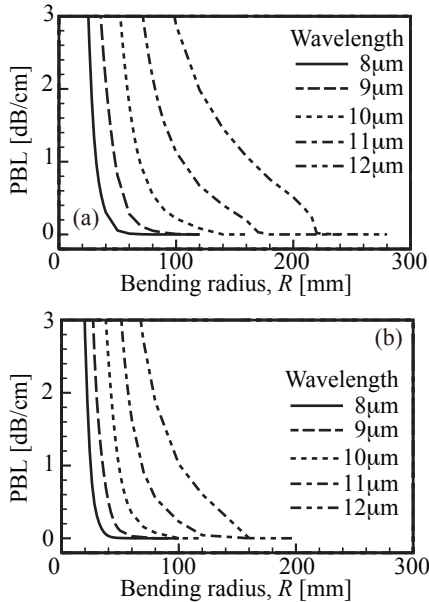
gular core. Evidently, operation at a longer wavelength requires a larger bending radius to suppress the PBL, and the rectangular waveguides show smaller PBLs than the square waveguides because of the stronger confinement of optical waves due to the relatively larger cross-sectional areas of the cores.

Figure 6 shows the DPL levels as functions of propagation distance for the square bent waveguides with bending radii are $R = 20$, 26, and 40 mm. Here, the refractive index changes, Δn, are 0.011, and the operation wavelengths are 8 μm. Total lengths of these bent waveguides are taken as $R\pi/2$. The DPL values reached steady-state levels at the ends of the waveguides. The
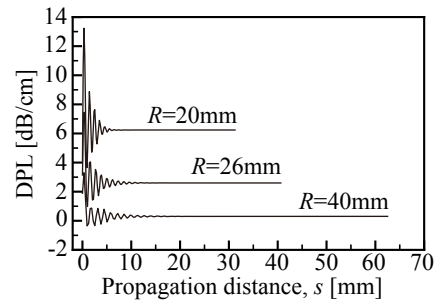

Fig. 6. Differential power loss (DPL) values of waveguides with $w = 15 \ \mu$m, $t = 15 \ \mu$m, and $\Delta n = 0.011$, at the wavelength of 8 μm for bending radii of 20, 26, and 40 mm.

Fig. 5. Pure bend loss as a function of bending radius for bent waveguides, whose refractive index change, Δn, of 0.011, with (a) $w = 15 \ \mu$m and $t = 15 \ \mu$m and (b) $w = 20 \ \mu$m and $t = 15 \ \mu$m.
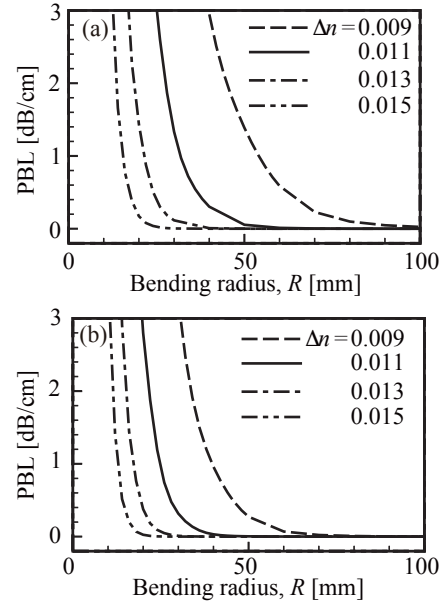

Fig. 7. Pure bend loss at a wavelength of 8 μm as a function of bend radius for bent waveguides with (a) $w = 15 \ \mu$m and $t = 15 \ \mu$m and (b) $w = 20 \ \mu$m and $t = 15 \ \mu$m.

oscillatory nature of the DPL is due to coupling from higher-order modes of the bent waveguide back into the fundamental mode of the straight waveguide[26].

Figure 7 shows the PBL as a function of bending radius at the wavelength of 8 μm for the square and the rectangular waveguides with $\Delta n = 0.009, 0.011, 0.013$, and 0.015. Evidently, the PBL strongly depends on the refractive index change, Δn. When the refractive index change decreases, the required bending radius rapidly increases to realize low-loss OICs.

As an practical example, we consider rectangular waveguides with $w = 20 \mu$m, $t = 15 \mu$m and $\Delta n = 0.013$, whose cross-sections are approximately identical to the fabricated waveguides[14]. Figure 7 (b) shows that the PBL of the waveguides are less than 1.2×10^{-3} dB/cm for $R > 36$ mm at the wavelength of 8.0 μm.

IV. CONCLUSION

In this study, the single-mode conditions and the bending loss characteristics of IG2-glass-based optical waveguides operating in the mid-IR spectral range are revealed. Guided-mode analysis was performed using a scalar FEM. As a result, the single-mode region was shown for the waveguide with $\Delta n = 0.011$ at the wavelength of 9 μm, is shown. In addition, the square and the rectangular waveguides, whose core widths and heights are in the single-mode region, were operated in a single-mode over the mid-IR spectral range. Two-dimensional ESW models of the bent waveguides were analyzed using a two-dimensional FD-BPM. The dependence of the loss characteristics on the waveguide parameters was investigated. Through ULI, the loss characteristics were found to strongly depend on the refractive index change, Δn.

ACKNOWLEDGMENT

REFERENCES

[1] A. N. Dinkelaker, A. Rahman, J. Bland-Hawthorn, F. Cantalloube, S. Ellis, P. Feautrier, M. Ireland, L. Labadie, and R. R. Thomson, "Astrophotonics: Introduction to the feature issue," *J. Opt. Soc. Am. B*, vol. 38, no. 7, pp. AP1-AP6, July 2021.

[2] J. Bland-Hawthorn and P. Kern, "Astrophotonics: A new era for astronomical instruments," *Opt. Express*, vol. 17, no. 3, pp. 1880-1884, Feb. 2009.

[3] J. Bland-Hawthorn and S. G. Leon-Saval, "Astrophotonics: Molding the flow of light in astronomical instruments," *Opt. Express*, vol. 25, no. 13, pp. 15549-15557, June 2017.

[4] S. Xie, J. Zhan, Y. Hu, Y. Zhang, S. Veilleux, J. Bland-Hawthorn, and M. Dagenais, "Add–drop filter with complex waveguide Bragg grating and multimode interferometer operating on arbitrarily spaced channels," *Opt. Lett.*, vol. 43, no. 24, pp. 6045-6048, Dec. 2018.

[5] A. S. Nayak, T. Poletti, T. K. Sharma, K. Madhav, E. Pedretti, L. Labadie, and M. M. Roth, "Chromatic response of a four-telescope integrated-optics discrete beam combiner at the astronomical L band," *Opt. Express*, vol. 28, no. 23, pp. 34346-34361, Nov. 2020.

[6] N. Cvetojevic, "Starlight on a chip: Astrophotonic technologies for interferometry," in P. G. Tuthill, A. Mérand, and S. Sallum, editors, *Optical and Infrared Interferometry and Imaging VII*, vol. 11446, p. 1144616, International Society for Optics and Photonics, SPIE, 2020.

[7] M.-A. Martinod, P. Tuthill, S. Gross, B. Norris, D. Sweeney, and M. J. Withford, "Achromatic photonic tricouplers for application in nulling interferometry," *Appl. Opt.*, vol. 60, no. 19, pp. D100-D107, July 2021.

[8] A. Benoît, F. A. Pike, T. K. Sharma, D. G. MacLachlan, A. N. Dinkelaker, A. S. Nayak, K. Madhav, M. M. Roth, L. Labadie, E. Pedretti, T. A. ten Brummelaar, N. Scott, V. C. du Foresto, and R. R. Thomson, "Ultrafast laser inscription of asymmetric integrated waveguide 3 dB couplers for astronomical K-band interferometry at the CHARA array," *J. Opt. Soc. Am. B*, vol. 38, no. 9, pp. 2455-2464, Sep. 2021.

[9] M. M. Roth, K. Madhav, A. Stoll, D. Bodenmüller, A. N. Dinkelaker, A. Rahman, E. Hernandez, A. Günther, and S. Vjesnica, "Astrophotonics: Photonic integrated circuits for astronomical instrumentation," in S. M. García-Blanco and P. Cheben, editors, *Integrated Optics: Devices, Materials, and Technologies XXVII*, vol. 12424, p. 124240B, International Society for Optics and Photonics, SPIE, 2023.

[10] M. Benisy, J.-P. Berger, L. Jocou, P. Labeye, F. Malbet, K. Perraut, and P. Kern, "An integrated optics beam combiner for the second generation VLTI instruments," *Astron. Astrophys.*, vol. 498, pp. 601-613, Oct. 2009.

[11] R. R. Thomson, A. K. Kar, and J. Allington-Smith, "Ultrafast laser inscription: An enabling technology for astrophotonics," *Opt. Express*, vol. 17, no. 3, pp. 1963-1969, Feb. 2009.

[12] J. E. McCarthy, H. T. Bookey, N. D. Psaila, R. R. Thomson, and A. K. Kar, "Mid-infrared spectral broadening in an ultrafast laser inscribed gallium lanthanum sulphide waveguide," *Opt. Express*, vol. 20, no. 2, pp. 1545-1551, Jan. 2012.

[13] A. Ródenas, G. Martin, B. Arezki, N. Psaila, G. Jose, A. Jha, L. Labadie, P. Kern, A. Kar,

and R. Thomson, "Three-dimensional mid-infrared photonic circuits in chalcogenide glass," *Opt. Lett.*, vol. 37, no. 3, pp. 392-394, Feb. 2012.

[14] H. L. Butcher, D. G. MacLachlan, D. Lee, R. R. Thomson, and D. Weidmann, "Ultrafast laser-inscribed mid-infrared evanescent field directional couplers in GeAsSe chalcogenide glass," *OSA Continuum*, vol. 1, no. 1, pp. 221-228, Sep. 2018.

[15] H. L. Butcher, D. G. MacLachlan, D. Lee, R. R. Thomson, and D. Weidmann, "Demonstration and characterization of ultrafast laser-inscribed mid-infrared waveguides in chalcogenide glass IG2," *Opt. Express*, vol. 26, no. 8, pp. 10930-10943, Apr. 2018.

[16] L. Labadie and O. Wallner, "Mid-infrared guided optics: A perspective for astronomical instruments," *Opt. Express*, vol. 17, no. 3, pp. 1947-1962, Feb. 2009.

[17] B. R. M. Norris, N. Cvetojevic, T. Lagadec, N. Jovanovic, S. Gross, A. Arriola, T. Gretzinger, M.-A. Martinod, O. Guyon, J. Lozi, M. J. Withford, J. S. Lawrence, and P. Tuthill, "First on-sky demonstration of an integrated-photonic nulling interferometer: The GLINT instrument," *Monthly Notices of the Royal Astronomical Society*, vol. 491, no. 3, pp. 4180-4193, Nov. 2019.

[18] N. Hô, M. C. Phillips, H. Qiao, P. J. Allen, K. Krishnaswami, B. J. Riley, T. L. Myers, and N. C. Anheier, "Single-mode low-loss chalcogenide glass waveguides for the mid-infrared," *Opt. Lett.*, vol. 31, no. 12, pp. 1860-1862, June 2006.

[19] Vitron, "IG2 datasheet," https://www.vitron.de/files/VITRON_IG-2_Datenblatt_Okt_2020__1_.pdf, Oct. 2020.

[20] W. Hu, M. Kilinc, W. Gebremichael, C. Dorrer, and J. Qiao, "Morphology and waveguiding properties of ultrafast-laser-inscribed type-II waveguides in IG2," *Opt. Mater. Express*, vol. 12, no. 1, pp. 360-373, Jan. 2022.

[21] M. Koshiba, *Optical Waveguide Theory by the Finite Element Method*, Tokyo, KTK Scientific Publishers, 1992.

[22] G. Pedrola, *Beam Propagation Method for Design of Optical Waveguide Devices*, John Wiley & Sons, 2015.

[23] M. Heiblum and J. Harris, "Analysis of curved optical waveguides by conformal transformation," *IEEE J. Quantum Electron.*, vol. 11, no. 2, pp. 75-83, Feb. 1975.

[24] K. Petermann, "Microbending loss in monomode fibers," *Electron. Lett.*, vol. 12, no. 4, pp. 107-109, Feb. 1976.

[25] J. Saijonmaa and D. Yevick, "Beam-propagation analysis of loss in bent optical waveguides and fibers," *J. Opt. Soc. Am.*, vol. 73, no. 12, pp. 1785-1791, Dec. 1983.

[26] R. Baets and P. E. Lagasse, "Loss calculation and design of arbitrarily curved integrated-optic waveguides," *J. Opt. Soc. Am.*, vol. 73, no. 2, pp. 177-182, Feb. 1983.

[27] Y. Nito, D. Kadowake, J. Yamauchi, and H. Nakano, "Bent embedded optical waveguide with a loaded metal film for reducing a polarization dependent loss," *J. Lightwave Technol.*, vol. 31, no. 19, pp. 3195-3202, Oct. 2013.

[28] G. R. Hadley, "Wide-angle beam propagation using Padé approximant operators," *Opt. Lett.*, vol. 17, no. 20, pp. 1426-1428, Oct. 1992.

[29] G. R. Hadley, "Transparent boundary condition for beam propagation," *Opt. Lett.*, vol. 16, no. 9, pp. 624-626, May 1991.

[30] J. Yamauchi, T. Ando, M. Ikegaya, and H. Nakano, "Effects of trench location on the attenuation constant in bent step-index optical waveguides," *IEICE Trans. Electron.*, vol. E77-C, no. 2, pp. 319-321, Feb. 1994.

[31] M. Rivera, "A finite difference BPM analysis of bent dielectric waveguides," *J. Lightwave Technol.*, vol. 13, no. 2, pp. 233-238, Feb. 1995.

[32] W. J. Song, G. Song, B. H. Ahn, and M. Kang, "Scalar BPM analyses of TE and TM polarized fields in bent waveguides," *IEEE Trans. Antennas Propag.*, vol. 51, no. 6, pp. 1185-1198, June 2003.

Takashi Yasui graduated with the B.S. degree in Electronic Engineering from Fukui University, Fukui, Japan, in 1997, and the M.S. and Ph.D. degrees in Electronic Engineering from Hokkaido University, Sapporo, Japan, in 1999 and 2001, respectively. From 1999 to 2002, he was a Research Fellow of the Japan Society for the Promotion of Science. In 2002, he joined Fujitsu Ltd., Chiba, Japan. From 2004 to 2011, he was an Assistant Professor of the Department of Electronic and Control Systems Engineering, Shimane University, Matsue, Japan. Since 2011, he has been an Associate Professor of the Faculty of Engineering, Kitami Institute of Technology, Kitami, Japan. He has been engaged in research on wave electronics. Yasui is a member of the IEEE, the Optica, and the Institute of Electronics, Information and Communication Engineers (IEICE) of Japan. In 2018, he was awarded the Excellent Paper Award from IEICE.